Pergamon

Int. J. Heat Mass Transfer. Vol. 38, No. 10, pp. 1813–1821, 1995

0017–9310/95 $9.50+0.00

0017–9310(94)00297–5

Development and application of an absorption-line blackbody distribution function for CO_2

M. K. DENISON and B. W. WEBB†

Department of Mechanical Engineering, Brigham Young University, Provo, UT 84602, U.S.A.

(*Received* 2 *November* 1993 *and in final form* 12 *September* 1994)

Abstract—An absorption-line blackbody distribution function for CO_2 is presented which permits efficient and accurate calculation of total heat transfer rates. The model allows the local absorption coefficient to be the basic radiative property, permitting its use in arbitrary solution methods of the radiative transfer equation (RTE). A mathematical correlation is presented to approximate the function for use in computer codes. Total emissivities calculated with the correlation agree well with Hottel data. Excellent agreement is also demonstrated with line-by-line solutions of the RTE.

INTRODUCTION

Radiative heat transfer in gases has important applications in atmospheric processes and combustion systems. The existing narrow-band models [1, 2] and wide-band models [3] provide spectrally integrated radiative properties (transmissivities, band absorptances, etc.) to make the strong spectral variation in gas radiation properties tractable to radiative transfer calculations. The spectral integration introduced by these models requires specification of a path-length *a priori* to evaluate the properties. The obvious choice of path-length may not exist in complex multidimensional media and/or situations which include scattering particulates and highly reflective boundaries. Line-by-line calculations do not require specification of a path-length to calculate the local monochromatic absorption coefficient. By specifying the absorption coefficient as the basic radiative property, the radiative transfer equation (RTE) may be solved in its fundamental form (in terms of an absorption coefficient) using arbitrary solution methods. However, due to many thousands of absorption lines that exist in the spectra of gases, line-by-line calculations are computationally expensive. Like line-by-line calculations, the k-distribution method [2, 4, 5] may, in its general formulation, be used in arbitrary solution methods of the RTE, but with great computational savings over line-by-line calculations. Direct application of k-distributions to obtain total heat transfer rates requires a quadrature over the absorption cross-section (k-space) for each narrow band where Planck's function may be assumed constant, followed by a quadrature over the bands.

Modest [6] has shown the weighted-sum-of-gray-gases (WSGG) model [7] to be applicable to the RTE written in terms of the absorption coefficient. In the absence of scattering the WSGG form of the RTE is written:

$$\frac{\mathrm{d}I_j}{\mathrm{d}s} = \kappa_j\left(a_j\frac{\sigma T^4}{\pi} - I_j\right). \tag{1}$$

Here, I_j, κ_j and a_j are the intensity, absorption coefficient, and corresponding weight associated with the jth gray gas. s is the distance along the given line of sight. The total heat transfer rates are found by simply summing the solutions of equation (1) over all gray gases:

$$I = \sum_j I_j. \tag{2}$$

Under the assumption of gray boundary conditions and particulates the WSGG model has greater computational efficiency than k-distributions in that only a single quadrature over the gas absorption cross-section is required to obtain total heat transfer rates. Denison and Webb [8] developed a spectral line-based WSGG model by constructing a histogram representation of the high-resolution spectra of H_2O. It was demonstrated in that paper that, when using relatively few gray gases, the optimum set of absorption cross-sections is dependent on the path-length range of the problem of interest. Therefore, this approach would require a histogram spectrum construction for each path-length range considered using detailed line-by-line data. It is desirable to obtain a correlation that contains the contribution of the continuous range of absorption cross-section so that any desired number of gray gases could be used. In a separate paper Denison and Webb [9] introduced a novel absorption-line blackbody distribution function for H_2O that easily allows any number of gray gases since the function is continuous in the absorption cross-section domain. Although that paper dealt with H_2O, the concepts presented may be applied to any radiatively active gas.

† Author to whom correspondence should be addressed.

NOMENCLATURE

a	blackbody weight of the WSGG model
I	radiation intensity
$\tilde{C}_{\text{abs},j}$	supplemental absorption cross-section
C_{abs}	absorption cross-section
E_{b}	blackbody emissive flux
F_{CO_2}	absorption-line blackbody distribution function for CO_2
L	path-length
P_{T}	total pressure
q	radiative heat flux
s	distance along line of sight
T	temperature
Y_s	mole fraction of species s.

Greek symbols

ε	total emissivity
η	wave number
κ	absorption coefficient
σ	Stephan–Boltzmann constant.

Subscripts

b	blackbody or blackbody source
g	gas
i	ith spectral segment
j	jth gray gas
loc	local
ref	reference
s	general species
w	wall
η	spectral.

In this paper an absorption-line blackbody distribution function and its correlation for CO_2 obtained from detailed spectra are presented. The detailed spectra were constructed from the Air Force Geophysics Laboratory's high-resolution transmission molecular absorption (HITRAN) data base [10] and from high temperature line estimates. The use of the function for efficient calculation of total radiative transfer from CO_2 is illustrated.

THE DISTRIBUTION FUNCTION

The absorption-line blackbody distribution function is defined as that fraction of the blackbody energy in the portions of the spectrum where the high-resolution spectral absorption cross-section of the gas $C_{\text{abs},\eta}$ is less than a prescribed value C_{abs} [9]. This is illustrated in Fig. 1 for a few absorption lines at high resolution. The portions of the spectrum over which Planck's function is integrated are represented by the shaded segments in the graph. The distribution function is then expressed as

$$F_{\text{CO}_2}(C_{\text{abs}},T_{\text{b}},T_{\text{g}},P_{\text{T}},Y_s) = \frac{1}{\sigma T_{\text{b}}^4}\sum_i \int_{\Delta\eta_i(C_{\text{abs}},T_{\text{g}},P_{\text{T}},Y_s)} E_{\text{b}\eta}(\eta,T_{\text{b}})\,\text{d}\eta \quad (3)$$

where σ is the Stephan–Boltzmann constant and $E_{\text{b}\eta}$ is Planck's function evaluated at the wave number η and blackbody (source) temperature T_{b}. The subscript i refers to the ith spectral segment and the summation is performed over all segments covering the entire spectrum. This fractional function has a monotonic increase between zero and unity with increasing absorption cross-section. The function is dependent on the absorption cross-section C_{abs}, blackbody source temperature T_{b}, gas temperature T_{g}, total pressure P_{T} and mole fraction of broadening species Y_s. The mathematical correlation of the function presented here is limited to one atmosphere pressure. The dependence of the function on the spectrum is through the spectral interval of integration of each segment $\Delta\eta_i$. It is useful to allow the function F_{CO_2} to depend on the two separate temperatures T_{g} and T_{b}. In total gas emissivity calculations of isothermal gaseous systems these temperatures are equivalent. However, in total absorptivity calculations they need not be the same, since the gas and the radiation source temperatures may differ.

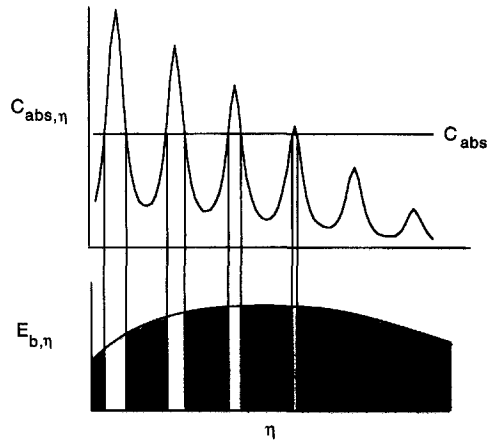

Fig. 1. Portions of the spectrum, for a few representative absorption lines, where the fraction of blackbody energy is calculated.

The fraction of the blackbody energy for a given source temperature in the spectral segments where the absorption cross-section is between arbitrary values $\tilde{C}_{\text{abs},j}$ and $\tilde{C}_{\text{abs},j+1}$ may be found simply as the difference of the distribution function evaluated at these two absorption cross-sections. These absorption cross-sections are called *supplemental* absorption cross-sections since they are used to determine the

blackbody weight but do not appear directly in the corresponding gray gas absorption coefficient κ_j. The difference of the distribution function evaluated at these supplemental cross-sections is the blackbody weight in the WSGG RTE [equation (1)]:

$$a_j = F_{CO_2}(\tilde{C}_{abs,j+1}, T_b, T_g, P_T, Y_s) - F_{CO_2}(\tilde{C}_{abs,j}, T_b, T_g, P_T, Y_s). \quad (4)$$

In a numerical calculation, the absorption cross-section domain is divided into discrete increments and a solution is carried out for each increment represented by a single value of the absorption cross-section or a single gray gas. The jth gray gas absorption coefficient is defined as the product $NC_{abs,j}$ where N is the molar density of the gas evaluated from an equation of state, and $C_{abs,j}$ is an appropriate mean value of the absorption cross-sectional area between $\tilde{C}_{abs,j}$ and $\tilde{C}_{abs,j+1}$. Denison and Webb [8] have shown for H_2O that good accuracy can be achieved with as few as three gray gases when the absorption cross-sections and supplemental absorption cross-sections are determined from an optimization involving total emissivities.

The function was calculated from detailed spectra of CO_2 with the same procedure outlined by Denison and Webb [9] for H_2O. Generation of the detailed spectra is outlined in the next section.

LINE-BY-LINE SPECTRA

In order to calculate the distribution function line-by-line data necessary for the construction of detailed spectra were taken from the 1991 version of the HITRAN database [10]. The Lorentz line profile, which is appropriate at atmospheric pressure [2] is used to describe each single spectral line. Including the overlap contribution of neighboring lines the absorption cross-section is written as

$$C_{abs,\eta} = \sum_i \frac{S_i}{\pi} \frac{\gamma_i}{(\eta-\eta_i)^2+\gamma_i^2} \quad (5)$$

where S_i is the integrated line intensity or strength of the ith line, γ_i is its half-width and η_i is its location. As in previous work the summation of equation (5) includes only neighboring lines for which the contribution to $C_{abs,\eta}$ is significant. All spectral lines within 25 cm^{-1} on either side of the wave number of interest η were included.

The HITRAN database was assembled for a gas temperature of 296 K. At sufficiently high temperatures the so-called "hot" lines which are not included in the database become significant. Therefore, the "hot" line parameters were obtained from the data given by Rothman *et al.* [11]. The line positions were obtained from the rotation vibration energy levels and the line half-widths were obtained from polynomial expressions [11]. Rotationless band intensities not given by Rothman *et al.* [11] were estimated using the procedure of Taine [12] for transitions in the radiatively participating non-degenerate mode of vibration, and Penner [13] for transitions involving the degenerate mode of vibration. It is recognized that this approach may yield errors in individual band intensities but, as will be shown later, yields total heat-transfer rates in good agreement with experimentally determined total emissivity data. The present work seeks to obtain an engineering model which will approximate the contribution of the entire spectrum efficiently in total radiative transfer calculations. The number of excited vibration levels considered accounts for at least 99.5% of the population of CO_2 molecules at thermodynamic equilibrium. A line intensity cutoff of 10^{-25} cm molec.$^{-1}$ was selected for the "hot" lines generated here. This cutoff was selected to be suited for path-lengths expected in high-temperature combustion applications.

DISTRIBUTION FUNCTION RESULTS

Figure 2 shows the absorption-line distribution function for CO_2 at the gas temperature of 1000 K and at the various blackbody source temperatures between 500 and 2500 K. Figure 2 shows the function at absorption cross-sections above 10^{-4} m^2 $mole^{-1}$ which is consistent with the cutoff of 10^{-25} cm molec.$^{-1}$ selected which covers the length ranges for practical high temperature applications. The function would reach a value of zero at C_{abs} below the overall minimum of the spectrum. As the source temperature is increased a given fraction of the blackbody energy is associated with a lower absorption cross-section. This is due to the presence of vibration bands whose strength generally decreases with increasing wave number and the nature of Planck's distribution moving toward higher wave numbers at higher temperatures. An exception to this trend occurs between the temperatures of 500 K and 1000 K at absorption cross-sections above 3 m^2 $mole^{-1}$. This reversal is due to the weaker bands below 1000 cm^{-1} as compared to the band at 2300 cm^{-1}.

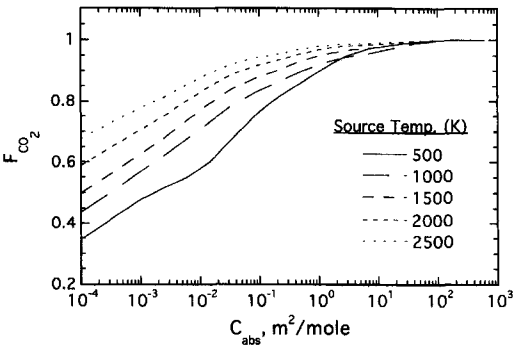

Fig. 2. The absorption-line blackbody distribution function for CO_2 calculated from a spectrum generated at a gas temperature of 1000 K.

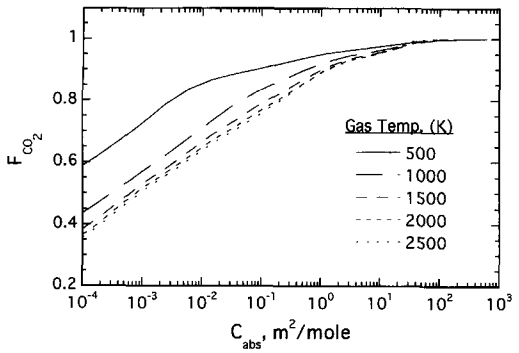

Fig. 3. The absorption-line blackbody distribution function for CO_2 calculated at a fixed blackbody source temperature of 1000 K from spectra generated at various gas temperatures.

Figure 3 shows the effect of fixing the blackbody source temperature at 1000 K and varying the gas temperature. As the gas temperature is increased, the number of absorption-lines that are significant increase, thereby reducing the fraction of the spectrum where $C_{\text{abs},\eta}$ is less than an arbitrary but fixed value C_{abs}. In Fig. 3 this is seen as a general decrease in the distribution function at a given C_{abs} with increasing gas temperature. For a fixed blackbody source temperature T_b, the gas becomes more absorbing with increasing gas temperature T_g. The distribution function is less sensitive to changes in gas temperature as the gas temperature is increased.

A RECOMMENDED MATHEMATICAL CORRELATION

The following hyperbolic tangent function similar to that used for H_2O [9] is recommended for CO_2:

$$F_{CO_2} = \tfrac{1}{2}\tanh\left[P(T_g, T_b, \xi)\right] + \tfrac{1}{2} \tag{6a}$$

where the function P is given as

$$P = \sum_{l=0}^{3}\sum_{m=0}^{3}\sum_{n=0}^{3} d_{lmn}\left(\frac{T_g}{2500}\right)^n\left(\frac{T_b}{2500}\right)^m \xi^l \tag{6b}$$

and

$$\xi = \ln\left(C_{\text{abs}}\right). \tag{6c}$$

T_g and T_b are in Kelvin and C_{abs} has the units m^2 $mole^{-1}$. The coefficients of the correlation d_{lmn}, found in Table 1, were determined from a least squares fit of the distribution function evaluated at 20 logarithmically spaced values of C_{abs} between 3×10^{-5} and 600 m^2 $mole^{-1}$, and at the same source and gas temperatures of 400, 500, 750, 1000, 1250, 1500, 1750, 2000, 2250 and 2500 K. Equation (6) is applicable to one atmosphere pressure. The quality of the fit is demonstrated in Fig. 4 where equation (6) is plotted against the actual data calculated from the line-by-line parameters at a gas temperature of 1000 K. It is recommended that the function not be used outside the gas temperature range of 400–2500 K since extrapolating any correlation beyond the data used in the fit is inappropriate. Caution should also be used with source temperatures above 2500 K. Emission temperatures below 400 K will not contribute significantly to any radiative calculation involving other gas regions or walls of higher temperature.

Although difficult to see in Fig. 4, the correlated fit approaches unity asymptotically whereas the actual absorption-line blackbody distribution function reaches unity just above 100 m^2 $mole^{-1}$. This asymptotic behavior of equation (6) results in an over-prediction of CO_2 absorption at very short path-lengths. This problem may be alleviated by lowering the upper limit of integration over the absorption cross-section domain from 600 to 120 m^2 $mole^{-1}$.

Unlike H_2O which is a strong self-broadener, the absorption-line distribution function for CO_2 is essentially independent of Y_{CO_2}. Hence, the correlation equation (6) has no such dependence. The actual small shift in the function due to self-broadening is well within the errors of the correlated fit.

VALIDATION

This section considers a few problems involving radiative transfer in CO_2 demonstrating the utility of the function. First, comparisons are made between Hottel emissivity data and emissivities calculated using the absorption-line distribution function presented here. Numerical solutions of the RTE with model properties as input are then considered. Comparisons between line-by-line benchmarks generated as part of this study and predictions from solutions of equation (1) demonstrate the accuracy of the function presented here. Problems were chosen to attempt to quantify the errors in the predicted radiative flux divergence using the present mathematical correlation of the distribution function over a range of optical depths. All the model predictions presented use equation (6). Comparisons with predictions using tabulated data from which the distribution function correlation was fit have shown no appreciable differences.

Comparison with Hottel emissivities

Figure 5 presents a comparison of Hottel total emissivity data [14] with total emissivities obtained using the WSGG expression for total emissivity given as

$$\varepsilon = \sum_j a_j\left(1 - e^{-\kappa_j L}\right). \tag{7}$$

Equations (4) and (6) were used to obtain the weights. The weights from previous WSGG models [15–17] have been found from an optimized fit with emissivity data as a function of path-length, temperature, and concentration, with only two or three terms in the summation. The calculation using equation (7) involved 20 gray gases in the summation with each discrete absorption cross-section determined as

Table 1. The coefficients d_{lmn} appearing in equation (6)

		$l = 0$		
m/n	0	1	2	3
0	2.45702	−5.45334	6.53751	−2.52344
1	−4.0232	15.67297	−24.3247	11.33757
2	7.54549	−23.8023	39.51896	−19.1137
3	−3.63104	11.9078	−20.3606	9.97877
		$l = 1$		
m/n	0	1	2	3
0	7.65678E-02	2.36184	−3.95061	2.17482
1	0.2901819	−12.0041	22.44342	−13.0467
2	−0.64282	21.5003	−40.8667	23.66762
3	0.3942158	−11.5818	22.05176	−12.6536
		$l = 2$		
m/n	0	1	2	3
0	−3.30582E-02	0.4367742	−0.725331	0.4138566
1	0.3672993	−3.52466	6.74885	−3.96295
2	−0.69811	6.60703	−12.9667	7.58713
3	0.3831158	−3.65683	7.19415	−4.16496
		$l = 3$		
m/n	0	1	2	3
0	−1.87927E-03	1.92123E-02	−3.25863E-02	1.98493E-02
1	2.85033E-02	−0.223537	0.4402715	−0.26267
2	−5.49594E-02	0.4370937	−0.881494	0.521958
3	3.04198E-02	−0.247793	0.4990777	−0.291566

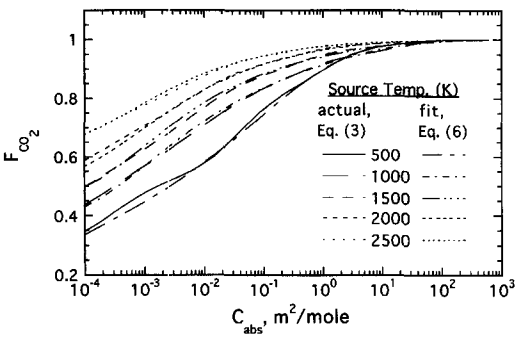

Fig. 4. Plot of equation (6) vs the actual calculated absorption-line blackbody distribution function of CO_2. T_g = 1000 K.

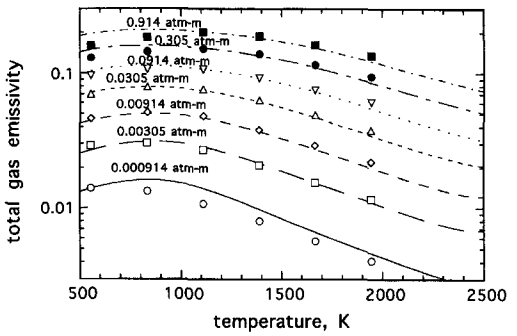

Fig. 5. Comparison between total emissivities of CO_2 from Hottel data (symbols) and emissivities calculated from equations (6)–(8) using 20 gray gases.

$$C_{\mathrm{abs},j} = \exp\left[\frac{\ln(\tilde{C}_{\mathrm{abs},j}) + \ln(\tilde{C}_{\mathrm{abs},j+1})}{2}\right]. \quad (8)$$

The absorption cross-section domain was divided into 20 logarithmically spaced intervals between 3×10^{-5} and 120 m^2 $mole^{-1}$. The total emissivities using the correlation are within 6% of the Hottel data at temperatures between 900 and 1600 K and at partial pressure path-lengths between 0.003 and 0.3 atm-m. At path-lengths less than 0.003 atm-m the error is as high as 30%. The error is generally within 12% at higher temperatures above 1600 K, except at partial pressure path-lengths below 0.003 atm-m (20% error) and above 0.3 atm-m (15% error). At temperatures below 600 K at longer path-lengths ($\geq$ 0.9 atm-m) the error is as high as 22%. An under-prediction of the total emissivity is apparent at temperatures above 1800 K. This is felt to be the result of too few cold band intensities available in the cold band data used

to estimate hot line parameters at high temperatures above 1800 K.

It is interesting to note that, unlike H_2O, the CO_2 total emissivity vs temperature shows a local maximum at about 900 or 1000 K. This maximum is due to the bands below 1000 cm^{-1} being less absorbing than the band at 2300 cm^{-1}. The H_2O bands on the other hand all decrease in strength with increasing wave number. The strongest H_2O band is the pure rotational band (no vibration transitions) at the far infrared (and microwave) portion of the spectrum. CO_2 has no pure rotational band since the molecule possesses no permanent electric dipole moment.

Solutions of the WSGG RTE

Solutions of the WSGG RTE [equation (1)] in one-dimensional geometry are next considered with the weights determined from equation (4) and the correlation of equation (6). In this work a simple discrete ordinates method is used applicable to a gray analysis described by Carlson and Lathrop [18] for solving a similar governing equation for neutron transport. The spatial grid in the calculations reported here has a resolution of between 40 and 120 grid points depending on the optical thickness of the medium for the particular problem. A nonuniform grid was used in order to accurately predict the flux divergence near a temperature discontinuity at a wall. For a one-dimensional geometry, an even-order Gauss quadrature set was used for the discrete ordinates. A quadrature order of 20 was chosen. This is the quadrature order used by Kim *et al.* [19] who reported no significant improvement with higher orders.

The model solutions are compared with line-by-line benchmarks. The benchmark predictions for validation of the distribution function presented above were generated by solving for the intensity field line-by-line using the detailed line data. Each of these computer runs involved between 80 000 and 200 000 spectral calculations. For each benchmark the actual high resolution spectrum was divided into 10 spectral regions between each pair of adjacent local maxima (perceptible lines), and a solution was carried out using the average absorption coefficient in each subline region. An increase in spectral resolution to 50 spectral calculations between adjacent local maxima showed no appreciable difference in the solution. For the case of a non-isothermal medium the spectrum at the highest temperature, which therefore had the greatest number of local maxima, was used as the basis for the spectral division just outlined. Each subline spectral region was held fixed throughout the spatial domain and the absorption coefficient was allowed to vary by determining the average absorption coefficient over the same subline region but from the spectrum at the local temperature and species concentration.

Figure 6 presents the prediction of the radiative flux divergence for uniform 20% CO_2 at 1000 K between infinite parallel walls spaced 0.1 m. The gray wall emissivities are 0.7 and 0.1 in Fig. 6(a) and (b), respectively. The total pressure is one atmosphere. The wall temperatures are 2000 and 300 K at $x = 0$ and 0.1 m, respectively. The figure presents the comparison between the benchmarks and the sum of solutions of equation (1) using three optimized gray gases and 20 non-optimized gray gases. The legend of Fig. 6 indicates the range of path-length over which optimization was performed in those simulations where optimization of the gray gas absorption cross-sections was used. The optimization procedure involved minimizing the squared relative error in emissivity, $(1-\varepsilon/\varepsilon_T)^2$, where ε and ε_T are determined by equation (7) using three gray gases and 20 gray gases, respectively. The optimization was carried out using discrete values of L over the path-length range indicated. In the 20-gray-gas solution to the RTE the supplemental absorption cross-sections were logarithmically spaced with the gray gas absorption cross-section of each gray gas determined from equation (8). The net radiative wall fluxes at the cold wall are also shown. In Fig. 6(a) the radiative flux divergence field predicted by the 20-gray-gas model is within 8% of the line-by-line benchmark. The optimized three-gray-gas results show the same agreement except at the hot wall where there is a discontinuity in temperature. The three-gray-gas predicted divergence at the wall is 20% lower than the benchmark. This is because the three-gray-gas-model is limited to a smaller range in the absorption cross-section than the 20-gray-gas-model. Close to the wall the divergence is changing rapidly with position. The net flux at the cold wall is within 3% of the benchmark. Figure 6(b)

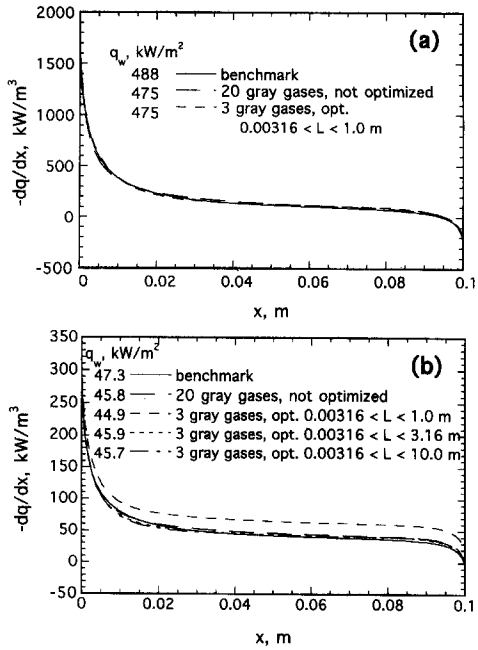

Fig. 6. Radiative flux divergence and cold wall net flux for 20% CO_2 at 1000 K. $T_{w,x=0} = 2000$ K. $T_{w,x=0.1m} = 300$ K. (a) $\varepsilon_w = 0.7$. (b) $\varepsilon_w = 0.1$. The three-gray-gas predictions are with optimized gray gas absorption cross-section.

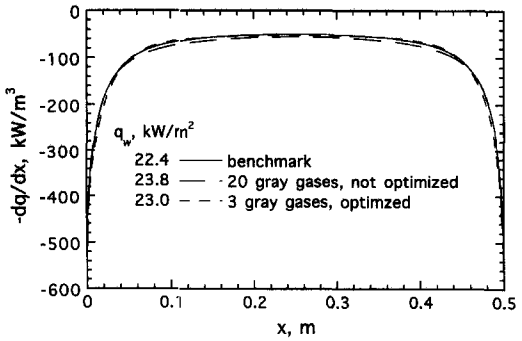

Fig. 7. Radiative flux divergence and cold wall net flux for 10% CO_2 at 1500 K. $\varepsilon_w = 1.0$. $T_w = 300$ K.

presents the results with highly reflective walls ($\varepsilon_w = 0.1$). Comparison between Fig. 6(a) and (b) shows a marked decrease in the radiative heat transfer rates which is not surprising given decreased wall emission. The 20-gray-gas solution exhibits excellent agreement with the benchmark solution. Using the same range in path-length in the optimization as was used in the predictions of Fig. 6(a) results in an over-prediction of the divergence profile. The optimized three-gray-gas solutions reveal that the range of path-length used in the optimization must be increased to achieve the same accuracy with highly reflecting walls. Interestingly, the upper limit on that path-length range required to achieve good accuracy is fully an order of magnitude higher than the relevant physical length of the system.

In Fig. 7, 10% CO_2 at 1500 K is radiating to infinite black walls spaced 0.5 m at 300 K. The model predicted flux divergence and net wall flux are within 10% of the benchmark. The better agreement in the predicted net wall flux of the three gray gas model with the benchmark (3% error) in comparison with 20 gray gases (6% error) is unexpected. This is felt to be due to compensating errors of the mathematical fit of equation (6) and the errors associated with using only three gray gases. Nevertheless the errors are in each case less than 10%.

Figure 8 demonstrates the model at a larger wall spacing of 5 m. The medium consists of 30% CO_2 at 1300 K. The walls are at 500 K with an emissivity of 0.9. The model predictions are again within 10% of the benchmark.

The required computation times for benchmark solutions of these isothermal problems were one to two hours on an HP 750 workstation. The WSGG calculations required less than one second CPU time which included the optimization for the three gray gas model. Hence, the economy in model predictions is illustrated with little loss in accuracy.

In non-isothermal, non-homogeneous media the method outlined by Denison and Webb [20] is used to determine the gray gas absorption cross-sections at each spatial location. This method (similar to the c–k method [2]) reveals an implicit dependence of the local gray gas absorption cross-section $C_{\mathrm{abs},j}$ on local temperature, composition and total pressure via equivalent absorption-line blackbody distribution functions at reference and local states

$$F_{CO_2}(C_{\mathrm{abs},j};\ T_b = T_{\mathrm{ref}};\ T_g = T_{\mathrm{loc}};\ Y_{CO_2} = Y_{CO_2,\mathrm{loc}};\ P_T = P_{T,\mathrm{loc}}) = F_{CO_2}(C_{\mathrm{abs},j,\mathrm{ref}};\ T_b = T_{\mathrm{ref}};\ T_g = T_{\mathrm{ref}};\ Y_{CO_2} = Y_{CO_2,\mathrm{ref}};\ P_T = P_{T,\mathrm{ref}}). \quad (9)$$

Implicit in equation (1) is the assumption that the spectral boundaries of the subline wave number segments associated with a single gray gas remain fixed throughout the problem spatial domain [8]. In non-uniform media the gas absorption spectrum varies with spatial location since integrated line intensities are known to depend on temperature, and half-widths are dependent on temperature and pressure. Therefore, when applying equation (4) to determine the blackbody weights, a single spectrum may be assumed for the entire domain as an assumption. This is accomplished by using a single reference value (a spatial average) of the gas temperature, mole fraction, and total pressure in the distribution function throughout the domain [20]

$$a_j = F_{CO_2}(\tilde{C}_{\mathrm{abs},j+1};\ T_b = T_{\mathrm{loc}};\ T_g = T_{\mathrm{ref}};\ Y_{CO_2} = Y_{CO_2,\mathrm{ref}};\ P_T = P_{T,\mathrm{ref}}) - F_{CO_2}(\tilde{C}_{\mathrm{abs},j};\ T_b = T_{\mathrm{loc}};\ T_g = T_{\mathrm{ref}};\ Y_{CO_2} = Y_{CO_2,\mathrm{ref}};\ P_T = P_{T,\mathrm{ref}}). \quad (10)$$

The blackbody source temperature can vary and is set to the local temperature. This is to account for the local distribution in the blackbody energy associated with volumetric emission. The molar density N also depends on the local temperature and composition.

Figure 9 illustrates the results of the above approach. Figure 9 shows the radiative source and net cold wall flux for a cosine temperature distribution given as

$$T = T_{\mathrm{ave}} + \frac{\Delta T}{2}\cos(\pi x/L). \quad (11)$$

The mole fraction of the CO_2 is spatially constant at

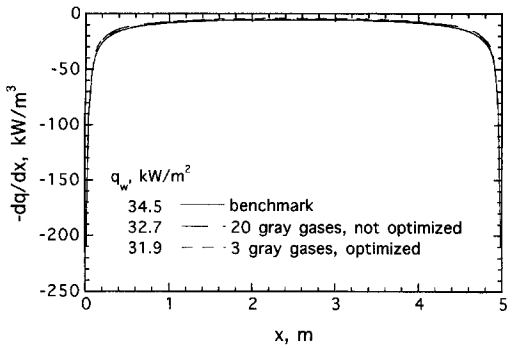

Fig. 8. Radiative flux divergence and cold wall net flux for 30% CO_2 at 1300 K. $\varepsilon_w = 0.9$. $T_w = 500$ K. $L = 5$ m.

a value of 0.3. The average temperature is 1250 K and $\Delta T = 1000$ K. The walls are again black and at the temperatures of 1750 and 750 K at $x = 0$ and 0.2 m, respectively. For comparison, a prediction is also shown in Fig. 9 with 20 gray gases of spatially constant absorption cross-section, $C_{\text{abs},j}$. The 20-gray-gas predicted flux divergence in the cold region is underpredicted by 17% in contrast to the 60% over-prediction assuming the absorption cross-section spectrum is spatially constant. The error trends show the same reversal as was seen with H_2O [20]. In the hot region the over-prediction of the radiative heat loss associated with the present approach is about 20% for 20 gray gases (not optimized), while the underprediction of spatially constant $C_{\text{abs},j}$ is 11%. Nevertheless, the errors overall are reduced by incorporating a spatial dependence of the absorption cross-sections. The divergence errors of the three-gray-gas (optimized) prediction are about 20% and 6% in the hot and cold regions, respectively. The predicted net cold wall flux is less than 2% for the 20- and three-gray-gas predictions compared to 3% error in the prediction assuming spatially constant $C_{\text{abs},j}$.

The computation time for the non-isothermal problem was roughly 140 h for the line-by-line benchmark on an HP 750 workstation. This is in sharp contrast to 3 s for the three-gray-gas solution including optimization and 10 s for the 20-gray-gas predictions. The sharp increase in the computation time of the benchmark is associated with evaluations of line-by-line properties at each spatial position.

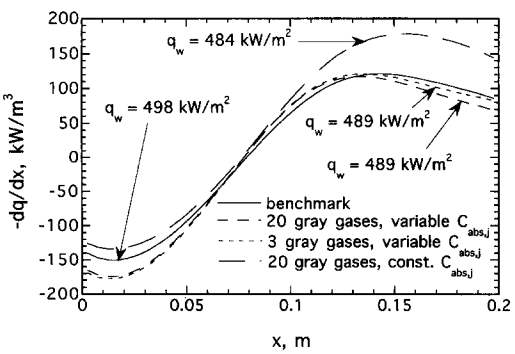

Fig. 9. Radiative source and net cold wall flux for the cosine temperature distribution [equation (11)] with 30% CO_2. $\Delta T = 1000$ K. $T_{\text{ave}} = 1250$ K. $T_{w,x=0} = 1750$ K. $T_{w,x=0.2\text{m}} = 750$ K. $\varepsilon_w = 1$.

The absorption-line blackbody distribution function presented here for CO_2 has also been applied to problems with non-gray boundaries and particulates [21]. Under these conditions, the approach involved the determination of weights by integrating Planck's function weighted by cumulative k-distributions over arbitrarily large bands. The radiative properties of the particulates and boundaries were assumed constant in these bands.

CONCLUSIONS

An absorption-line blackbody distribution function for CO_2 has been presented which lends itself to efficient total radiative transfer calculations compared to line-by-line as well as narrow band calculations. A mathematical correlation has been presented which has been shown to provide predictions generally within 10% of line-by-line predictions for isothermal media. Approximate solutions may also be obtained for non-isothermal media. Total emissivities calculated from the function compare well with experimental Hottel data.

Acknowledgements—This work was supported by the Advanced Combustion Engineering Research Center (ACERC) at Brigham Young University. ACERC is sponsored by the National Science Foundation, the State of Utah, the U.S. Department of Energy, and a number of industrial participants. One of the authors (MKD) also wishes to acknowledge the financial support of the NASA Rocky Mountain Grant Consortium.

REFERENCES

1. C. B. Ludwig, W. Malkmus, J. E. Reardon and J. A. L. Thompson, *Handbook of Infrared Radiation from Combustion Gases*, NASA SP-3080, Scientific and Technical Information Office, Washington, DC (1973).
2. R. M. Goody and Y. L. Yung, *Atmospheric Radiation* (2nd Edn). Clarendon Press, Oxford (1989).
3. D. K. Edwards, Molecular gas band radiation, *Adv. Heat Transfer* **12,** 115–193. Academic Press, New York (1976).
4. A. Arking and K. Grossman, The influence of line shape and band structure on temperatures in planetary atmospheres, *J. Atmos. Sci.* **29,** 937–949 (1972).
5. G. A. Domoto, Frequency integration for radiative transfer problems involving homogeneous non-gray gases: the inverse transmission function, *J. Quant. Spectrosc. Radiat. Transfer* **14,** 935–942 (1974).
6. M. F. Modest, The weighted-sum-of-gray-gases model for arbitrary solution methods in radiative transfer, *ASME J. Heat Transfer* **113,** 650–656 (1991).
7. H. C. Hottel and A. F. Sarofim, *Radiative Transfer*. McGraw-Hill, New York (1967).
8. M. K. Denison and B. W. Webb, A spectral line-based weighted-sum-of-gray-gases model for arbitrary RTE solvers, *ASME J. Heat Transfer* **115,** 1004–1012 (1993).
9. M. K. Denison and B. W. Webb, An absorption-line blackbody distribution function for efficient calculation

of total gas radiative transfer, *J. Quant. Spectrosc. Radiat. Transfer* **50,** 499–510 (1993).
10. L. S. Rothman, R. R. Gamache, R. H. Tipping, C. P. Rinsland, M. A. H. Smith, D. Chris Benner, V. Malathy Devi, J. M. Flaud, C. Camy-Peyret, A. Perrin, A. Goldman, S. T. Massie and L. R. Brown, The HITRAN molecular database: editions of 1991 and 1992, *J. Quant. Spectrosc. Radiat. Transfer* **48,** 469–507 (1992).
11. L. S. Rothman, R. L. Hawkins, R. B. Wattson and R. R. Gamache, Energy levels, intensities, and linewidths of atmospheric carbon dioxide bands, *J. Quant. Spectrosc. Radiat. Transfer* **48,** 537–566 (1992).
12. J. Taine, A line-by-line calculations of low-resolution radiative properties of CO_2–CO–transparent non-isothermal gases mixtures up to 3000 K, *J. Quant. Spectrosc. Radiat. Transfer* **30,** 371–379 (1983).
13. S. S. Penner, *Quantitative Molecular Spectroscopy and Gas Emissivities*. Addison–Wesley, Reading, Massachusetts (1959).
14. H. C. Hottel, In *Heat Transmission* (3rd Edn) (Edited by W. H. McAdams), Chap. 4. McGraw-Hill, New York (1954).
15. T. F. Smith, Z. F. Shen and J. N. Friedman, Evaluation of coefficients for the weighted sum of gray gases model, *ASME J. Heat Transfer* **104,** 602–608 (1982).
16. A. Coppalle and P. Vervisch, The total emissivities of high-temperature flames, *Combustion Flame* **49,** 101–108 (1983).
17. P. B. Taylor and P. J. Foster, The total emissivities of luminous and non-luminous flames, *Int. J. Heat Mass Transfer* **17,** 1591–1605 (1974).
18. B. G. Carlson and K. D. Lathrop, Transport theory—the method of discrete ordinates. In *Computing Methods in Reactor Physics* (Edited by H. Greenspan, C. N. Kelber and D. Okrent), Chap. 21. Gordon & Breach, New York (1968).
19. T. K. Kim, J. A. Menart and H. S. Lee, Nongray radiative gas analyses using the S–N discrete ordinates method, *ASME J. Heat Transfer* **113,** 946–952 (1991).
20. M. K. Denison and B. W. Webb, The spectral line-based weighted-sum-of-gray-gases model in non-isothermal non-homogeneous media, *ASME J. Heat Transfer* (in press).
21. M. K. Denison and B. W. Webb, *k*-Distributions and weighted-sum-of-gray-gases—a hybrid model, *Heat Transfer*—1994, **2,** 19–24 (1994).